The Antarctic Circumpolar Current in Equilibrium

BLANCA GALLEGO

Department of Atmospheric Sciences, University of California, Los Angeles, Los Angeles, California

PAOLA CESSI

Scripps Institution of Oceanography, University of California, San Diego, La Jolla, California

JAMES C. MCWILLIAMS

Department of Atmospheric Sciences, University of California, Los Angeles, Los Angeles, California

(Manuscript received 26 November 2002, in final form 21 January 2004)

ABSTRACT

A simple channel-flow model is used to examine the equilibrium upper-ocean dynamics and thermodynamics of the Antarctic Circumpolar Current (ACC). The model consists of two zonally averaged, variable-temperature layers—a surface boundary layer and a thermocline layer—separated by a turbulent interface. Weak air–sea heat flux, determined by relaxation to a prescribed atmospheric temperature, determines the leading-order temperature structure in the oceanic surface layer. The equilibrium thermal structure in the interior is mostly determined by a dominant balance between the meridional transport due to the wind-driven Eulerian mean circulation and the heat flux due to the baroclinic eddies. The resulting latitudinal temperature gradient depends on both the wind and the atmospheric temperature forcing and sustains the geostrophic zonal flow. Consideration of the next-order balance for the oceanic surface temperature results in an air–sea heat flux proportional to the magnitude of the residual flow. The residual meridional circulation (Eulerian mean plus eddy-induced) is necessary to balance small diabatic sources and sinks of heat. Therefore, it depends on the processes of vertical diffusion, boundary layer entrainment/detrainment, and, on the polar flank, convection. In the absence of substantial lateral diffusion, the leading-order balance of weak residual circulation implies a very weak meridional heat transport across the ACC and a correspondingly weak differential heat exchange to the atmosphere. This limitation can be eased if the lateral diffusive flux of temperature in the surface layer becomes as large as the adiabatic eddy transport.

1. Introduction

Knowledge of the dynamics and thermodynamics of the Antarctic Circumpolar Current (ACC) and its interaction with the atmosphere above, the sea ice, and the waters at lower latitudes is essential for understanding the earth's climate. Although substantial progress has been made in observations of the Southern Ocean during the last decade, we still do not have a complete picture of the ACC system. Perhaps the most important missing pieces are a reliable description of the meridional transport (including transport by eddies) and a good estimate of the air–sea heat and freshwater fluxes. The meridional velocities are too small to be measured directly and need to be inferred from a combination of hydrographic and altimetry data, wind measurements, and estimates of the air–sea heat and freshwater fluxes (see, e.g., Deacon 1984; Schmitz 1996; Speer et al. 2000; Rintoul et al. 2001). Meanwhile, air–sea fluxes have been estimated using in situ measurements from the Comprehensive Ocean–Atmosphere Dataset (COADS; daSilva et al. 1994). However, poor spatial and temporal coverage over the Southern Ocean as well as large errors in the observing procedure make these estimates unreliable. For instance, the air–sea heat flux estimated from COADS is of the order of 10 W m^{-2} over the Southern Ocean while exhibiting an overall global imbalance of 30 W m^{-2} and systematic errors of the order of 15 W m^{-2} (see Josey et al. 1999). Also, COADS estimate has a dubious local ocean warming around 45°S. On the other hand, air–sea heat fluxes derived from National Centers for Environmental Prediction (NCEP) and European Centre for Medium-Range Weather Forecasts (ECMWF) reanalyses are on the order of 20 W m^{-2} and do not exhibit a local warming (see Trenberth et al. 2001). Trenberth et al. (2001) show that, unlike the derived NCEP and ECMWF surface fluxes, those from

Corresponding author address: Paola Cessi, Scripps Institution of Oceanography, University of California, San Diego, 9500 Gilman Drive, MC 0213, La Jolla, CA 92093-0213.
E-mail: pcessi@ucsd.edu

COADS do not give reasonable implied northward oceanic heat transports.

The absence of continental barriers along the ACC path imparts this region with dynamical balances different from those at other latitudes. Both wind and buoyancy forcing affect the latitudinal density gradient that sustains the zonal flow. The equilibration of the ACC takes place through (i) a tilting of the isopycnals by the wind-driven Ekman flow, (ii) an opposing tilting by the mesoscale baroclinic eddies, and (iii) water transformation by diabatic fluxes of heat and freshwater.

The important role played by the baroclinic eddies in the redistribution of momentum and buoyancy within the ACC system has long been recognized (see, e.g., McWilliams et al. 1978; Johnson and Bryden 1989; Gent et al. 1995; Ivchenko et al. 1996; Marshall 1997; Marshall et al. 2002; Karsten et al. 2002). Consequently, the transformed Eulerian mean (TEM) formulation, traditionally applied to the zonally averaged dynamics of the atmosphere (see Andrews et al. 1987), has proven to be useful in the study of the ACC. It illustrates the two competing mechanisms of meridional transport: the Eulerian mean circulation, directly forced by the wind, and the eddy-induced circulation, which is how eddies release the potential energy of the system. The meridional circulation, given by the sum of Eulerian mean plus eddy-induced velocity, has been called the residual circulation. In the absence of diabatic terms, whether inside the domain or through boundary fluxes, the residual circulation is exactly zero. For the special case of zero residual circulation and quasigeostrophic dynamics, a standard parameterization of downward eddy flux of potential vorticity yields to a scaling of the baroclinic transport as a function of the strength of the wind stress and the magnitude of the background stratification. The specific scaling law depends on the choice of the eddy diffusivity. A summary of several such scaling estimates can be found in Rintoul et al. (2001).

However, a description of the equilibrium state (or long-term evolution) of the ACC must include the effects of the sources and sinks of buoyancy and, in particular, the link to the air–sea buoyancy fluxes. The way in which mechanical and thermodynamical balances combine to set the stratification and transport in the ACC system is still a subject of much debate. General circulation models have explored some of the aspects of the combined wind–buoyancy effects in the ACC zonal transport and meridional overturning (Cai and Baines 1996; Gnanadesikan and Hallberg 2000; Gent et al. 2001). These numerical results reveal a strong connection between the response of the ACC to mechanical forces and the response to thermohaline forces. However, these models contain complex information related to the interactions of the Southern Ocean with the cryosphere, the topography, and the rest of the ocean's circulation. Therefore, simple models of channel flows may be useful for achieving a clear picture of the equilibrium dynamics of the ACC.

Recently, Karsten et al. (2002) and Marshall and Radko (2003, hereinafter MR) have used the TEM formulation to make estimates of the stratification, transport, and meridional overturning circulation resulting from a thermally and mechanically driven circumpolar flow. In MR the strength of the residual streamfunction is determined by the thermodynamic balance in a surface mixed layer of prescribed buoyancy distribution and surface buoyancy flux. The slope of the isopycnals is computed from the vertically integrated TEM zonal momentum equation in an adiabatic interior. Scaling estimates of the stratification and baroclinic transport are obtained in the limit of zero residual streamfunction. An analogous ocean model had been previously used by Marshall (1997) to describe eddy-induced subduction of water masses in the Southern Ocean and its relationship with the surface buoyancy. Solutions of these models of the ACC dynamics are very useful to visualize the competing role of the wind and the eddies in setting the buoyancy distribution in the ocean's interior. However, because both the surface buoyancy distribution and the surface buoyancy flux are prescribed, these models do not give any information about the influence of the ocean's interior, either in the surface buoyancy field or in the residual circulation. In Karsten et al. (2002), the assumption of a zero-order balance between the mean and the eddy-induced circulations is also used to advance scaling arguments in the context of circumpolar dynamics. In their work, the residual circulation is related to both the surface buoyancy and a prescribed surface buoyancy flux. Their major scaling assumption results in a residual circulation proportional to the windstress.

Two important missing pieces in the prediction of the buoyancy distribution and the meridional overturning in the ACC are 1) air–sea buoyancy fluxes, which are not prescribed but settled internally taking ocean dynamics into account, and 2) the effects of internal diabatic processes in the determination of the residual circulation. The present model includes these effects in an idealized model of the zonally averaged, large-scale dynamics of the upper ocean. This work focuses on the local role of the ACC in the energy budget when there is no exchange of mass and buoyancy across the lateral boundaries.

The ACC is not zonal but meanders, steered by bottom topography. However, except from some curvature terms, a zonal average is formally equivalent to a streamwise average, that is, an average along the streamlines instead of along latitudinal circles (Ivchenko et al. 1996). Our model consists of a thermocline layer and a surface boundary layer separated by a turbulent interface. Each layer is characterized by horizontally variable temperature and thickness. For simplicity, the contribution of salinity to the equation of state has been ignored. This makes the model solutions less realistic but we believe it does not change the basic understanding of the qualitative role played by the buoyancy bal-

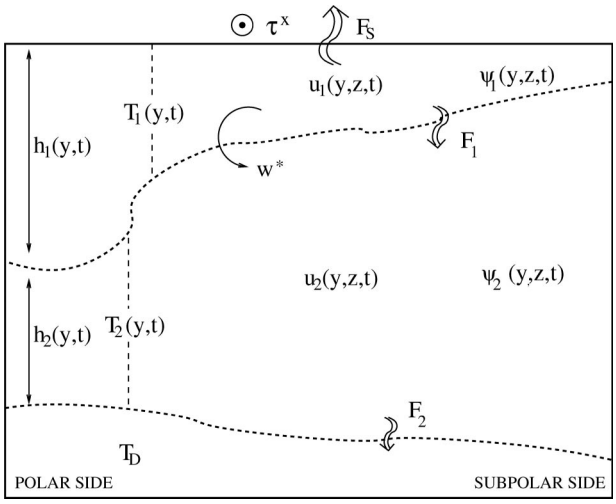

FIG. 1. Sketch of the model.

ances. A description of the model is contained in section 2, and section 3 presents the main features of the model solutions. Section 4 describes the equilibrium thermal distribution, corresponding zonal transport, and the equilibrium residual overturning and its associated air–sea heat flux. At the end of section 4 there is an analysis of the role of horizontal diffusion in the surface layer.

2. Model

We model the large-scale, upper-ocean dynamics and thermodynamics of a channel flow using a zonally averaged, variable temperature two-layer formulation, sketched in Fig. 1. It consists of a surface boundary layer of variable temperature, $T_1(y, t)$, and variable thickness, $h_1(y, t)$, above a thermocline layer of variable temperature, $T_2(y, t)$, and variable thickness, $h_2(y, t)$. Below the thermocline, the ocean has a constant temperature, T_D. At the interface $z = -h_1$ turbulent entraintment may occur while the interface $z = -h_1 - h_2$ is a material surface. Similar layered models of the ocean with lateral density gradients have been used in previous work (see, e.g., McCreary and Lu 1994).

In each layer, i, the temperature and layer thickness evolve in time according to the zonally averaged heat and mass equations:

$$\partial_t T_i + (v_i + v_i^{\text{eddy}})\partial_y T_i = \frac{Q_i}{h_i} \quad \text{and}$$

$$\partial_t h_i + \partial_y(h_i v_i + h_i v_i^{\text{eddy}}) = -(-1)^{(i)} w^*. \qquad (1)$$

Here, v_i is the zonally averaged meridional velocity, while v_i^{eddy} is the zonally averaged eddy-induced flow due to unresolved baroclinic eddies; Q_i includes the diabatic heating processes and w^* is the entraintment velocity representing diabatic mixing.

a. Large-scale circulation

The large-scale horizontal velocities are determined by the Boussinesq momentum balance,

$$f(-v_i, u_i) = -\frac{1}{\rho_o}(0, \partial_y p_i) + \mathbf{A}_i. \qquad (2)$$

Here, f is the Coriolis parameter, ρ_o is a reference density, p_i are the pressures, and $\mathbf{A}_i$ represents mechanical forcing and friction defined by

$$\mathbf{A}_1 = \frac{1}{h_1\rho_o}(\tau^x, 0) - \frac{1}{h_1}\left(r_x \int_{-h_1}^{0} u_1\, dz,\ r_y \int_{-h_1}^{0} v_1\, dz\right) \qquad (3)$$

and

$$\mathbf{A}_2 = -\frac{1}{h_2}\left(r_x \int_{-h_1-h_2}^{-h_1} u_2\, dz,\ r_y \int_{-h_1-h_2}^{-h_1} v_2\, dz\right), \qquad (4)$$

where τ^x is the wind stress associated with the atmospheric westerlies. The smaller meridional component of the wind stress is neglected. The friction coefficients r_x, r_y represent an inverse time scale for velocity decay due to friction.

Because the pressure is hydrostatic and the temperature is piecewise constant in depth, the geostrophic zonal flow is linear in depth within each layer,

$$u_{g1} \equiv -\frac{\partial_y p_1}{f\rho_o}$$

$$= -\frac{g\alpha_o}{f}\partial_y[(T_2 - T_D)h_2 + (T_1 - T_D)(h_1 + z)] \qquad (5)$$

and

$$u_{g2} \equiv -\frac{\partial_y p_2}{f\rho_o} = -\frac{g\alpha_o}{f}\partial_y[(T_2 - T_D)(h_2 + h_1 + z)]. \qquad (6)$$

Here, $\alpha_o = \rho^{-1}\partial\rho/\partial T$ is the thermal expansion coefficient and g is the gravitational acceleration.

The total zonal flow is linear in z within each layer and is mainly geostrophic:

$$u_1 = u_{g1} + \frac{\gamma}{h_1}\left(-r_x r_y \int_{-h_1}^{0} u_{g1}\, dz - r_y\frac{\tau^x}{\rho_o}\right) \quad \text{and}$$

$$u_2 = u_{g2} + \frac{\gamma}{h_2}\left(-r_x r_y \int_{-h_1-h_2}^{-h_1} u_{g2}\, dz\right), \qquad (7)$$

while the meridional velocities are constant in z within each layer:

$$v_1 = \frac{\gamma}{h_1}\left(r_x f \int_{-h_1}^{0} u_{g1}\, dz - f\frac{\tau^x}{\rho_o}\right) \quad \text{and}$$

$$v_2 = \frac{\gamma}{h_2}\left(r_x f \int_{-h_1-h_2}^{-h_1} u_{g2}\, dz\right). \qquad (8)$$

Here, $\gamma \equiv (f^2 + r_x r_y)^{-1}$.

The meridional streamfunction, ψ_i, can be computed from $\partial_z\psi_i = -v_i$ with the following boundary condi-

tions—1) it vanishes at the surface, $\psi_{1[z=0]} = 0$; 2) it is equal to the total meridional transport at the bottom, $\psi_{2(z=-h_1-h_2)} = v_1h_1 + v_2h_2$; and 3) it is continuous across the interface $z = -h_1$, $\psi_{1(z=-h_1)} = \psi_{2(z=-h_1)}$:

$$\psi_1 = -zv_1 \quad \text{and}$$

$$\psi_2 = -(z + h_1 + h_2)v_2 + (h_1v_1 + h_2v_2). \tag{9}$$

This streamfunction represents an overturning circulation in the meridional plane with water forced by the wind moving in the upper layer and returning in the lower layers. A transport given by $-h_1v_1 - h_2v_2$ is implied in the deep ocean: assuming a very deep ocean, its velocity is weak and the dynamical coupling to the upper ocean is negligible.

b. Eddy-induced circulation

The effect of mesoscale eddies in the ocean has been included by introducing an eddy velocity field that mixes temperature and layer thickness while transporting heat adiabatically (it can be eaily shown that in each layer the heat between two isopycnals is not modified by the effect of the eddy transport). The eddy-induced velocities are parameterized as a function of the resolved fields. The effect of baroclinic eddies on the mean variables is a poleward advection of mean buoyancy and a downward transfer of mean zonal momentum through interfacial form stress (see, e.g., Gent et al. 1995; Treguier et al. 1997), such that potential energy is released by flattening the isopycnals. Therefore, v_i^{eddy} must be such that the eddies' heat transport decreases the zonally averaged potential energy of the system. The potential energy is given by

$$\overline{\text{PE}} \equiv \int_{-h_1-h_2}^{0}\int_{0}^{L_y} \frac{g\rho}{2\rho_o}\, z\, dy\, dz$$

$$= \frac{g\alpha_o}{2}\int_0^{L_y} [(T_2 - T_D)(h_1 + h_2)^2 + (T_1 - T_2)h_1^2]\, dy, \tag{10}$$

where L_y is the width of the channel. The component of the variation of $\overline{\text{PE}}$ due to the eddies is

$$\frac{d^{\text{eddy}}}{dt}\overline{\text{PE}} = -\frac{g\alpha_o}{2}\int_0^{L_y} \partial_y[(T_2 - T_D)(h_1 + h_2)(h_1v_1^{\text{eddy}} + h_2v_2^{\text{eddy}})] - \frac{g\alpha_o}{2}\int_0^{L_y} \partial_y[(T_1 - T_2)h_1(h_1v_1^{\text{eddy}})]\, dy$$

$$+ \frac{g\alpha_o}{2}\int_0^{L_y} (h_1v_1^{\text{eddy}} + h_2v_2^{\text{eddy}})\left[(T_2 - T_D)\partial_y(h_1 + h_2) + \frac{h_2}{2}\partial_y(T_2 - T_D)\right] dy$$

$$+ \frac{g\alpha_o}{2}\int_0^{L_y} h_1v_1^{\text{eddy}}\left[(T_1 - T_2)\partial_y h_1 + \frac{(h_1 + h_2)}{2}\partial_y(T_2 - T_D) + \frac{h_1}{2}\partial_y(T_1 - T_2)\right] dy. \tag{11}$$

Therefore, with $v_i^{\text{eddy}} = 0$ at the lateral boundaries, a choice for the eddy transport that guarantees a decrease in the potential energy is

$$(h_1v_1^{\text{eddy}} + h_2v_2^{\text{eddy}}) = -\nu_2\left[\partial_y(h_1 + h_2) + \frac{h_2}{2}\frac{\partial_y(T_2 - T_D)}{(T_2 - T_D)}\right] \quad \text{and} \tag{12}$$

$$(h_1v_1^{\text{eddy}}) = -\nu_1\left[\partial_y h_1 + \frac{(h_1 + h_2)}{2}\frac{\partial_y(T_2 - T_D)}{(T_1 - T_2)} + \frac{h_1}{2}\frac{\partial_y(T_1 - T_2)}{(T_1 - T_2)}\right], \tag{13}$$

where ν_1 and ν_2 are positive constant eddy diffusivities. The meridional eddy-induced stream-function, ψ_i^{eddy}, is computed from the eddy-induced velocity, v_i^{eddy}, in the same way as the streamfunction of the Eulerian mean.

In a zonally averaged formulation, a decrease of the potential energy of the system implies ψ^{eddy} proportional to $\partial_y b$, where b stands for the zonally averaged buoyancy. In order to decrease $\overline{\text{PE}}$, ψ^{eddy}, should be proportional to $\partial_y b$ in z coordinates; for example, $\psi^{\text{eddy}} = -\nu(\partial_y b/\partial_z b)$ (Treguier et al. 1997). In isopycnal coordinates, $\overline{\text{PE}}$ decrease if $\psi^{\text{eddy}} = -\nu(\partial_y h/h)$, where h is the zonally averaged isopycnal depth. In our model, the buoyancy gradient at a given point in z, and therefore the parameterization of ψ^{eddy}, depends on both $\partial_y T$ and $\partial_y h$. This results from the particular choice of vertical temperature profile.

The input of momentum by the surface wind stress, τ^x/ρ_o, is mostly balanced by isopycnal form stress against the inert, deep ocean. In the zonally averaged, zonal momentum equation integrated over the upper ocean, this term is contained in the Coriolis force, $f\int_{-h_1-h_2}^{0} v\, dz = -f\int_{-h_1-h_2}^{0} v^{\text{eddy}}\, dz$.

c. Diabatic heating

The term Q_i in (1) represents the vertically integrated diabatic sources and sinks of heat within each layer. It is given by

$$Q_i = F_{\text{top}\,i} - F_{\text{bot}\,i} + \partial_y(\kappa_i h_i \partial_y T_i) - (T_1 - T_2)w^* H[-(-1)^i w^*]. \quad (14)$$

The term $F_{\text{top}\,i} - F_{\text{bot}\,i}$ is the net vertical heat flux into layer i; $F_{\text{top}\,1}$ is the air–sea heat flux (which will be called F_s) and it has been parameterized using a standard linear bulk formula,

$$F_s = \frac{\lambda}{C_{\text{po}}\rho_o}(T_{\text{as}} - T_1), \quad (15)$$

where C_{po} is the oceanic specific heat; λ is the bulk transfer coefficient, assumed constant; and T_{as} is the apparent equilibrium temperature of the atmosphere at the surface; $F_{\text{top}\,2} = F_{\text{bot}\,1}$ and $F_{\text{bot}\,2}$ (which will be referred to as F_1 and F_2, respectively) represent vertical diffusion of heat and consist of two parts, a downgradient diffusion term with constant diffusivities μ_i and a convective adjustment term:

$$F_1 = \mu_1\left(\frac{1}{h_1} + \frac{1}{h_2}\right)(T_1 - T_2) + \text{CA} \quad \text{and}$$

$$F_2 = \mu_2\left(\frac{1}{h_2} + \frac{1}{H_D}\right)(T_2 - T_D) + \text{CA}. \quad (16)$$

The convective adjustment (CA) acts at the bottom of each layer when the temperature jump is smaller than some minimum temperature difference, δT, which is positive because not all restratification processes are resolved by the model.

The last term in (14) represents the heat exchange at the base of the surface boundary layer due to entrainment. When w^* is positive, there is cooling in the upper layer while, when w^* is negative, there is heating in the lower layer. Also Q_i contains lateral diffusivity terms, $\partial_y(\kappa_i h_i \partial_y T_i)$. In the thermocline layer, the redistribution of temperature by the mesoscale, adiabatic eddies is much larger than that due to lateral diffusion. Therefore, the diffusivity coefficient κ_1 will be always taken to be much smaller than that of the adiabatic eddies, ν_1.

d. Entrainment–detrainment parameterization

Close to the ocean surface, the effect of turbulent eddies in the momentum and heat transport becomes very significant. The main sources of turbulent energy are the mechanical stirring by the wind and the mixing induced by convective instability due to cooling of the sea surface by the atmosphere. The penetration of these turbulent effects into the ocean is halted by the gain of potential energy due to entrainment of denser fluid from the lower layers.

Traditionally, boundary layer models consist of an evolution equation for the layer's depth with short time responses. Layer deepening occurs at a rate calculated from some turbulent-energy balance (see, e.g., Kraus and Turner 1967). However, an equilibrium climate model, such as the one presented here, requires a steady-state boundary layer depth. A useful simplified parameterization relates w^* to the rate of relaxation of h_1 toward an equilibrium surface layer depth, h_1^{eq},

$$w^* = \frac{1}{t_{\text{adj}}}(h_1^{\text{eq}} - h_1). \quad (17)$$

Here, t_{adj} is a constant adjustment time that represents the relaxation to the low-frequency equilibrium depth. It encompasses the time scales of mechanical and convective mixing and dissipation. The equilibrium depth, h_1^{eq}, is estimated as that obtained with the background stratification and wind-induced boundary layer shear such that a critical value of a bulk Richardson number is maintained (see, e.g., Zilitinkevich and Mironov 1996),

$$h_1^{\text{eq}} = \left[C_o \frac{2}{g\alpha_o} \frac{u^{*2}}{(T_1 - T_2)(1/h_1 + 1/h_2)}\right]^{1/2}, \quad (18)$$

where C_o is an a dimensional constant and u^* is the turbulent velocity defined as

$$u^{*2} = u_{\text{ls}}^2 + u_{\text{ss}}^2 \quad (19)$$

with $u_{\text{ls}}^2 = |\tau^x|/\rho_o$. Here, u_{ls} is the surface friction velocity of the large-scale wind, and u_{ss} is a constant velocity which accounts for the subgrid scales of the wind forcing and the surface currents.

3. Climatology of a control run

The model equations (1) are integrated in time to a steady state within a channel of width L_y. Here, y increases northward from $y = 0$ at the poleward side of the channel to $y = L_y$ at the equatorward side. Since the channel is in the Southern Hemisphere, $f < 0$. The β-plane approximation has been used and $f = -f_o + \beta(y - L_y/2)$.

The lateral boundary conditions are $v_i = 0$ and $\partial_y T_i = 0$. In addition, ν_i vanishes at the boundaries, so there is no exchange of mass or heat there. The locations of the subpolar and polar boundaries approximately coincide with zeros of the meridional Ekman flux. For simplicity we choose to neglect any upper-ocean meridional heat flux there, but there is an implicit meridional flux involved in maintaining the deep ocean temperature at T_D. The channel width is $L_y = 4500$ km, but we include regions of flat atmospheric forcing close to the lateral walls in order to avoid any spurious boundary effect. The meridional extent of the ''forced'' ocean is 2700 km. The prescribed atmospheric forcings plotted in Fig. 2 are idealized forms of the westerlies and of the latitudinal surface temperature gradient over the ACC. The model is started with a stratified ocean at rest, but the final state is independent of the initial configuration.

The parameter values in the control run are listed in Table 1. The value of the deep ocean temperature, T_D

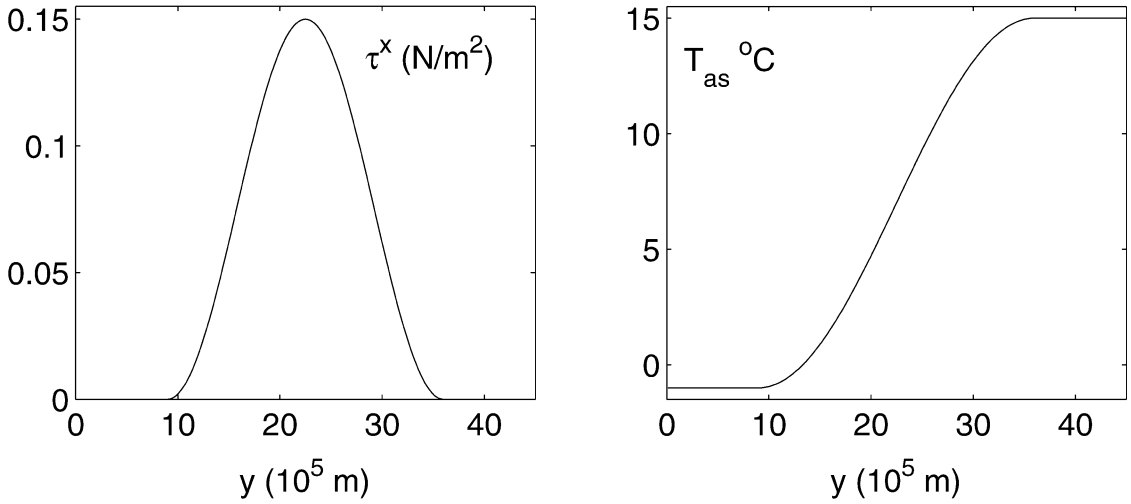

FIG. 2. Atmospheric forcing: (left) wind stress and (right) surface temperature.

$= -3.0$°C, is somewhat artificial, but it ensures that deep convection (convection below layer 2) is not part of the steady-state solution. However, this is not the case for some extreme parameter values explored in section 4. The minimum allowed temperature difference between layers, before convection takes place, is $\delta T = 0.5$°C. The parameters controlling the entrainment rate ensure an average surface layer depth of about 300 m for standard values of the stratification and turbulent velocity. The relaxation time is $t_{\text{adj}} = 180$ day, chosen to be just longer than the unresolved seasonal cycle and much smaller than the typical time scales of the resolved oceanic processes. The corresponding entrainment rate is about 2×10^{-7} m s^{-1} in the center of the channel, which is one order of magnitude smaller than the typical Ekman pumping of $\partial_y \tau^x/(\rho_o f_o) \sim 2 \times 10^{-6}$ m s^{-1}. The other parameters are typical of the ACC.

The steady-state oceanic temperature, shown in the left panel of Fig. 3, is characterized by isolines that slope upward to the pole outcropping at the surface. In the surface layer, the oceanic temperature follows the atmospheric forcing and decreases southward from 15° to -1°C, with a maximum gradient of $(9.4 \times 10^{-3}$ °C km^{-1} located at the center of the channel. In the thermocline layer, the ocean temperature decreases southward from 11° to -1.5°C. It has a maximum gradient of 8.7×10^{-3} °C km^{-1} located slightly northward from the maximum gradient of surface temperature. The stratification, $(T_1 - T_2)(h_1^{-1} + h_2^{-1})$, is of the order of 24°C km^{-1}, at the center of the channel and collapses to a minimum value, $\delta T(h_1^{-1} + h_2^{-1}) = 2.25$°C km^{-1}, at the poleward boundary. Although highly truncated in the vertical, the temperature field contains the basic features found in the southern upper ocean (see e.g., Gordon et al. 1982; Olbers et al. 1992).

The zonal flow, shown in the right panel of Fig. 3, decreases linearly with depth following a thermal-wind law with a small discontinuity at the layers interface. Its meridional maximum coincides with the largest gradient of the thermocline temperature. The total transport of 102 Sv (Sv $\equiv 10^6$ m^3 s^{-1}) is consistent with the upper-ocean fraction of the observed total transport. Estimates for Drake Passage transport are of the order of 135 Sv (Nowlin and Klinck 1986), with the most recent ones (from mooring measurements) describing an equivalent barotropic zonal flow with an *e*-folding depth of about 700 m (Gille 2003).

The air–sea heat flux, shown in Fig. 4, is characterized by weak ocean cooling everywhere except at the subpolar boundary where warming balances the entrainment cooling. The air–sea heat flux has a small positive average accounting for the heat lost through diffusion with the deep ocean.

Meridional overturning

The mean meridional circulation of the ACC (often called the Deacon cell) has water in the Ekman layer

TABLE 1. Parameter values for the control run.

$T_D = -3.0$°C	$g = 10$ m s^{-2}	$(\kappa_1, \kappa_2) = (10, 1)$ m^2 s^{-1}
$C_{po} = 3985$ J kg^{-1} °C^{-1}	$\alpha_o = 1.36 \times 10^{-4}$ °C^{-1}	$(\mu_1, \mu 2) = (5.0, 5.0) \times 10^{-6}$ m^2 s^{-1}
$\rho_o = 1027.5$ kg m^{-3}	$r_x = 0.05$ day^{-1}	$(\nu_1, \nu_2) = (1300, 1300)$ m^2 s^{-1}
$\delta T = 0.5$°C	$r_y = 0.05$ day^{-1}	$t_{\text{adj}} = 180.0$ day
$\lambda = 25.0$ W m^{-2} °C^{-1}	$f_o = 9.0$ day^{-1}	$C_o = 4000$
$H_D = 4000$ m	$\beta = 1.6 \times 10^{-5}$ m^{-1} day^{-1}	$H = 1000$ m
$L_x = 20 \times 10^6$ m	$L_y = 4 \times 10^6$ m	$u_{ss} = 1.0 \times 10^{-2}$ m s^{-1}

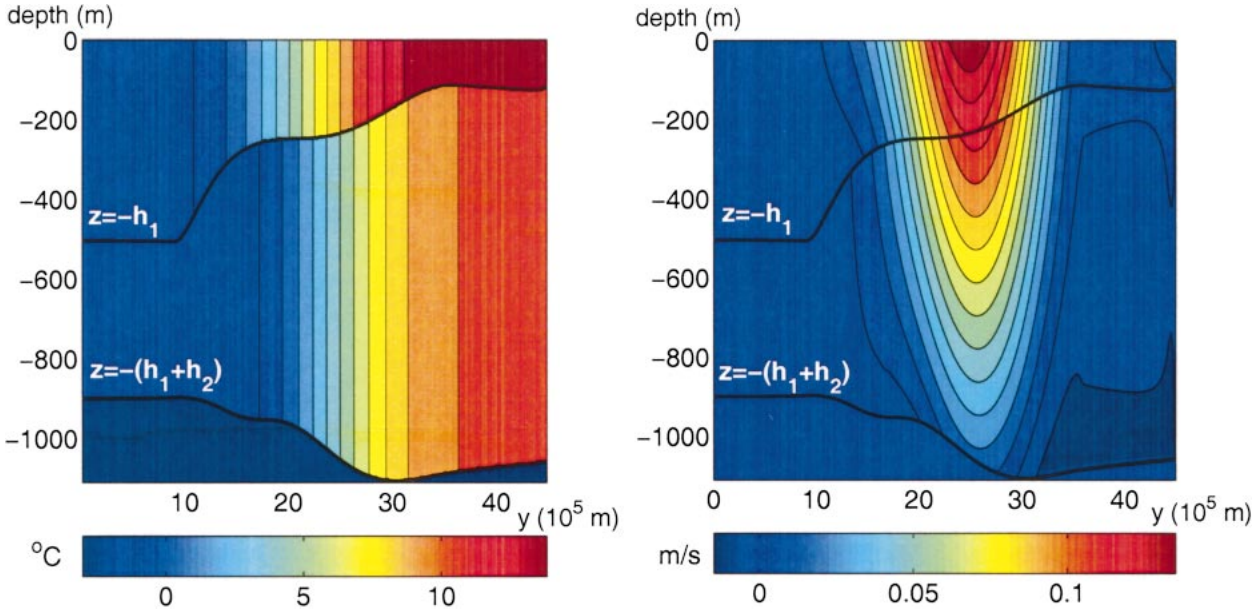

FIG. 3. (left) Oceanic temperature and (right) zonal flow for the control run.

transported equatorward by the wind and returned at depth by Reynolds stresses and frictional processes. In the present model, the equatorward transport takes place in the surface layer and the poleward subsurface flow is partitioned between the thermocline and the deep ocean. In the thermocline, this flow is proportional to the meridional temperature gradient and to the damping parameter r_x. The streamfunction of this meridional cell, plotted in the upper-left panel of Fig. 5, has a maximum amplitude of 24.9 Sv, very close to the 25 Sv estimate obtained using the the annual mean wind stress data from the Southampton Oceanography Centre (Karsten and Marshall 2002). The corresponding meridional velocity in our model has a maximum of 0.50 cm s^{-1}.

The streamfunction corresponding to the eddy-induced meridional circulation, plotted in the upper-right panel of Fig. 5, has the same order of magnitude as the mean meridional overturning and the opposite sign. It peaks at −25.6 Sv and the fastest eddy-induced velocity is −0.53 cm s^{-1}. Heat is advected in the meridional plane by the sum of the mean and eddy-induced overturning, called the residual circulation. In steady state, the transport of heat by the residual meridional flow balances the diabatic heating [cf. (1)]. For the special case of a conservative heat balance, $Q_i = 0$, the residual circulation is exactly zero. The lower panel of Fig. 5 shows the streamfunction of the residual circulation, $\psi_i^R = \psi_i + \psi_i^{\text{eddy}}$, corresponding to our control run. The eddy-induced velocities exceed the mean velocities at all latitudes, and the residual circulation transports heat poleward. In the surface layer, the warming of the southern latitudes is balanced by heat loss on the poleward side relative to the equatorward side due to the air–sea heat flux. In the lower layer, the cooling of the northern latitudes is balanced by heat gain on the equatorward side relative to the poleward side due to vertical diffusion and detrainment warming. At the center of the channel, where the wind stress is strongest, the Deacon cell almost balances the eddy-induced cell, and the resulting residual flow is very small. The residual circulation peaks at the side of the channel where the wind stress, and therefore the Deacon cell, goes to zero. The residual circulation has a double-cell structure with one cell occupying the equatorward half of the channel and a narrower cell at the polar flank. The corresponding local peaks are −3.0 Sv for the equatorward side and −1.8 Sv for the poleward side. This double-peak pattern remains fairly robust throughout the parameter space of this model. Only in the case of weak winds, the local maximum

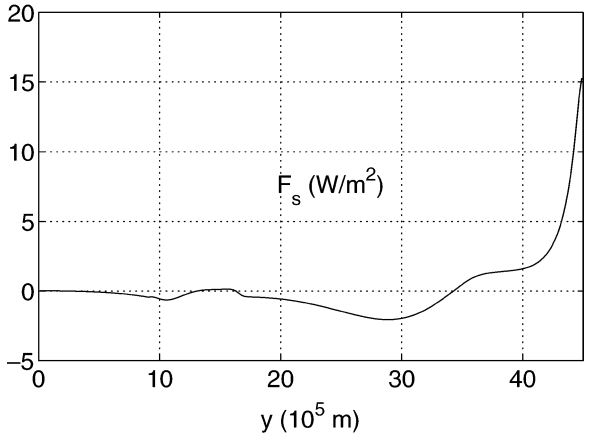

FIG. 4. Air–sea heat flux for the control run.

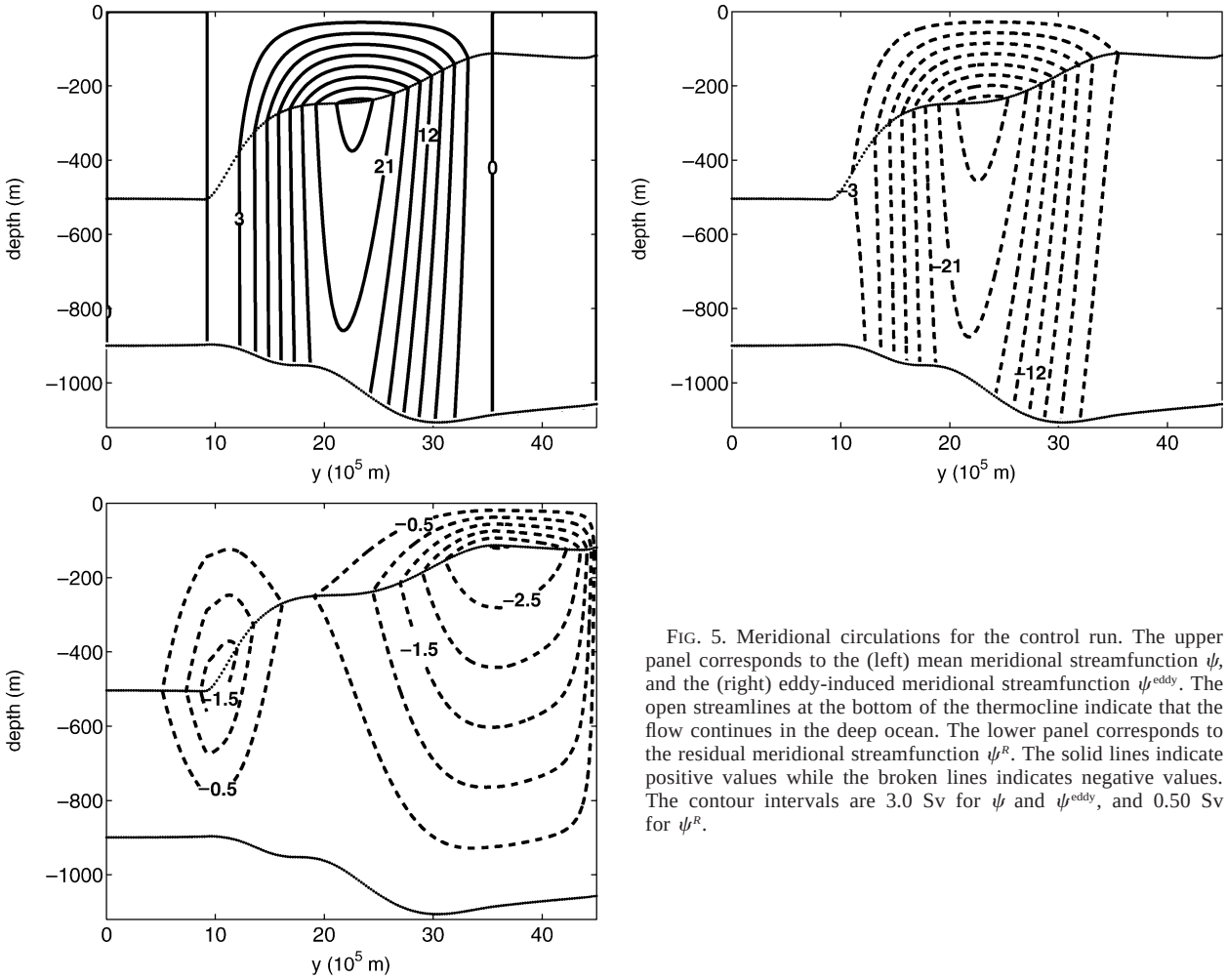

FIG. 5. Meridional circulations for the control run. The upper panel corresponds to the (left) mean meridional streamfunction ψ, and the (right) eddy-induced meridional streamfunction ψ^{eddy}. The open streamlines at the bottom of the thermocline indicate that the flow continues in the deep ocean. The lower panel corresponds to the residual meridional streamfunction ψ^R. The solid lines indicate positive values while the broken lines indicates negative values. The contour intervals are 3.0 Sv for ψ and ψ^{eddy}, and 0.50 Sv for ψ^R.

at the polar flank disappears and the channel is occupied by a single cell. Furthermore, it will be shown in section 4 that each cell is due to different physical processes and that some set of parameter values can produce a residual circulation in which the cell on the subpolar flank changes sign.

A similar cancellation between the mean and the eddy-induced meridional overturning has been found in eddy-resolving numerical models. Doos and Webb (1994) explored the meridional cells of the Southern Ocean using FRAM (Fine Resolution Antarctic Model). They found that zonal integration along density layers produced the virtual disappearance of the Deacon cell. The remaining meridional cells involved flows in and out of the northern boundary. A leading-order balance between the mean and eddy-induced circulations was also observed in a high-resolution numerical model of a circumpolar flow in Karsten et al. (2002) and accompanying laboratory experiments in Marshall et al. (2002). Deacon cell near cancellation is a characteristic of oceanic global climate models (GCMs) with the Gent and McWilliams (1990) mesoscale eddy parameterization (Danabasoglu et al. 1994; Gent et al. 2001).

In the absence of lateral diffusion, the leading-order balance of zero residual meridional flow implies a very weak poleward heat transport across the Southern Ocean. For the control run, shown in Fig. 6, the horizontal heat transport peaks at about 6×10^{13} W and it is mostly balanced by cooling to the atmosphere.

4. Parameter dependences and scaling estimates

Now we determine the sensitivities of the temperature and velocity fields of the equilibrium ACC to the atmospheric forcing and to the parameters controlling the internal dynamical processes. First we describe the thermal structure and its corresponding geostrophic zonal transport by using the leading order balances of zero air–sea heat flux, zero residual circulation, and zero entrainment rate. Then we analyze the next order balance for the meridional residual circulation and its corresponding air–sea heat flux.

a. Surface temperature

The first important thermodynamical result is a consequence of relaxing the surface ocean temperature to a prescribed atmospheric temperature. There are several time scales associated with the physical processes that distribute heat in the surface layer, namely, advection ($t_{\rm adv}$), relaxation to a prescribed atmospheric temperature ($t_{\rm rlx}$), horizontal diffusion ($t_{\rm hd}$), and vertical diffusion ($t_{\rm vd}$):

$$\underbrace{-(\Psi + \Psi^{\rm eddy})\partial_y T_1}_{\rm adv} \underbrace{- \partial_y(\Psi + \Psi^{\rm eddy})(T_1 - T_2)H(w^*)}_{\rm adv} + \underbrace{\frac{\lambda}{C_{\rm po}\rho_o}(T_{\rm as} - T_1)}_{\rm rlx} + \underbrace{\partial_y(\kappa_1 h_1 \partial_y T_1)}_{\rm hd}$$
$$\underbrace{- \mu_1\left(\frac{1}{h_1} + \frac{1}{h_2}\right)(T_1 - T_2)}_{\rm vd} = 0. \tag{20}$$

Here Ψ and $\Psi^{\rm eddy}$ refer, respectively, to the value of ψ and $\psi^{\rm eddy}$ at $z = -h_1$ and correspond to the vertically integrated transports in the surface layer. For the regime under consideration $\nu_1 \sim 1300$ m^2 s^{-1}, $\lambda \sim 25$ W m^{-2} °C^{-1}, $\kappa_1 \sim 10$ m^2 s^{-1}, and $\mu_1 \sim 5 \times 10^{-6}$ m^2 s^{-1}. The advective time scale is estimated with the Ekman transport $\Psi \sim 25$ Sv so that

$$t_{\rm adv} \sim 9.5 \text{ yr}, \qquad t_{\rm rlx} \sim 1.5 \text{ yr},$$
$$t_{\rm hd} \sim 7000 \text{ yr}, \quad \text{and} \quad t_{\rm vd} \sim 600 \text{ yr}. \tag{21}$$

Clearly the fastest time scale is $t_{\rm rlx}$ and the leading-order balance for the heat equation at the surface is

$$F_s \equiv \frac{\lambda}{C_{\rm po}\rho_o}(T_{\rm as} - T_1) \sim 0$$

so that

$$T_1 \sim T_{\rm as}. \tag{22}$$

b. Thermocline temperature

In the thermocline layer, the heat balance is given by

$$\underbrace{(\Psi + \Psi^{\rm eddy})\partial_y T_2}_{\rm adv} \underbrace{- \partial_y(\Psi + \Psi^{\rm eddy})(T_1 - T_2)H(-w^*)}_{\rm adv} + \underbrace{\partial_y(\kappa_2 h_2 \partial_y T_2)}_{\rm hdint} + \underbrace{\mu_1\left(\frac{1}{h_1} + \frac{1}{h_2}\right)(T_1 - T_2)}_{\rm vd}$$
$$\underbrace{- \mu_2\left(\frac{1}{h_2} + \frac{1}{H_D}\right)(T_2 - T_D)}_{\rm vddeep} = 0. \tag{23}$$

With $\nu_2 \sim \nu_1$, $\kappa_2 \sim 0.1 \times \kappa_1$, and $\mu_2 \sim \mu_1$ the diffusive time scales are

$$t_{\rm hdint} \sim 70\,000 \text{ yr} \quad \text{and} \quad t_{\rm vddeep} \sim 6000 \text{ yr}. \tag{24}$$

It is clear that no diabatic term in (23) can balance the advection of heat by the mean or the eddies individually, whose time scale is $t_{\rm adv}$ estimated in (21). The leading order balance is between the mean and the eddy induced circulations; that is,

$$\Psi \sim -\Psi^{\rm eddy}. \tag{25}$$

Since the mean transport is mostly given by the Ekman circulation and the dominant contribution to the eddy transport comes from the latitudinal gradient of the thermocline temperature, we may approximate (25) by

$$-\frac{\tau^x}{f\rho_o} \sim \nu_1 \frac{(h_1 + h_2)\partial_y T_2}{2(T_1 - T_2)}. \tag{26}$$

This relation provides a scaling for the slope of the isopycnals due to the competing effects of the wind forcing and the eddy tilting.

Estimating the total depth of the upper ocean, $h_1 + h_2$, with its volume-averaged value, H (which must be conserved), using the central value of the Coriolis parameter, $-f_o$, and the peak value of the wind stress, τ^x_o, we

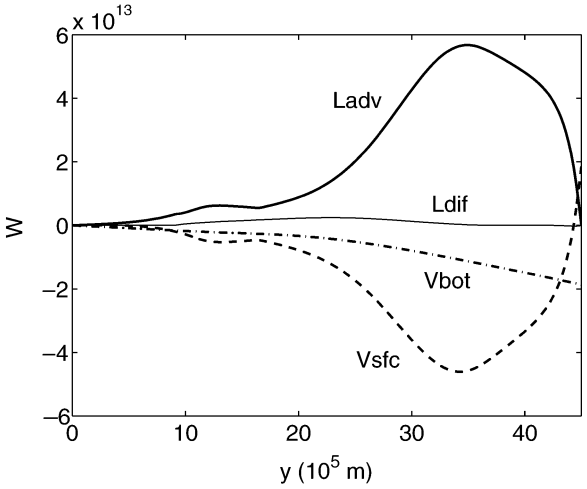

FIG. 6. Meridional heat transport for the control run. The thicker solid line (Ladv) and thinner solid line (Ldif) refer to the transport by the residual circulation and the horizontal diffusion respectively. The broken line (Vsfc) and mixed dot–solid line (Vbot) refer to the differential heating due to the vertical heat flux at the surface and the vertical heat flux at the bottom, respectively.

obtain the following scaling relation for the typical isopycnal slope over the center of the channel

$$\frac{(h_1 + h_2)\partial_y T_2}{T_1 - T_2} \sim \frac{H}{L_d} \tag{27}$$

with $L_d \equiv H\nu_1 f_o \rho_o / 2\tau_o^x$. Here L_d is a dynamical length of the system that reflects the competing effects of the wind and the eddies in the tilting of the isopycnals. Using typical values for the wind stress of 0.15 N m^{-2} and for the eddy diffusivity of 1300 m^2 s^{-1}, we find $L_d \sim 500$ km. In a continuously stratified thermocline with a downgradient parameterization of the eddy heat flux, the assumption of a leading order balance between the mean and the eddy-induced circulations results in the isopycnal's slope $\partial_y T/\partial_z T \sim \tau_o^x/(\nu f_o \rho_o)$, where ν is the eddy diffusivity parameter. Expression (27) is simply this scaling applied to our vertical discretization.

The horizontal length scale of the thermocline temperature is set by the scale of the prescribed atmospheric temperature, L_a so that

$$\frac{\partial_y T_2}{T_2 - T_D} \sim \frac{\partial_y T_{\text{as}}}{T_{\text{as}} - T_D} = \frac{1}{L_a}. \tag{28}$$

Combining (22), (27), and (28) we obtain a leading-order expression for the latitudinal variation of T_2 and for the vertical temperature difference $(T_1 - T_2)$, given by

$$\partial_y T_2 \sim \partial_y T_{\text{as}} \frac{L_a}{L_d + L_a} \quad \text{and}$$

$$(T_1 - T_2) \sim (T_{\text{as}} - T_D)\frac{L_d}{L_d + L_a}. \tag{29}$$

The three major mechanisms that affect the latitudinal and vertical temperature gradient are included in (29): the tilting of the isopycnals by the wind-driven Ekman flow, the opposing tilting by the mesoscale baroclinic eddies, and the water transformation at the surface. In the limit of $L_a \gg L_d$, the thermocline temperature would be entirely determined by the atmospheric surface temperature, $\partial_y T_2 \sim \partial_y T_{\text{as}}$. In the limit of $L_d \gg L_a$, the thermocline temperature would increase linearly with τ_o^x/ν_1, $\partial_y T_2 \sim [2\tau_o^x(T_{\text{as}} - T_D)]/(Hf_o\rho_o\nu_1)$. Typical values of $L_d \sim 500$ km are of the same order of magnitude as the length scale imposed by the forcing, $L_a \sim 1000$ km. We conclude that in the central region of the channel, where the residual circulation is small, the thermocline temperature is set by the atmospheric temperature, modified by the effect of the wind–eddy balance, which makes $\partial_y T_2$ grow toward the value $\partial_y T_{\text{as}}$, and $(T_1 - T_2)$ decrease toward $(T_{\text{as}} - T_D)$, with increasing winds and decreasing eddy activity.

Figures 7a–c show the values of $\partial_y T_i$ (upper panels) integrated over the interval $y = 1500$ km to $y = 3000$ km and for different values of the magnitude of the wind stress (a), of the eddy diffusivity (b), and of the atmospheric temperature gradient (c). All the variables have been normalized by their corresponding solution-set averages. The asterisks and circles correspond to the model solutions while the lines correspond to (22) and (29), predicted by the scaling theory. Both the atmospheric temperature gradient and the wind stress have been varied by changing their amplitude while conserving their simple forms depicted in Fig. 2.

The vertical scale of penetration of the surface temperature gradient that characterizes the thermocline layer is $h_E \sim HL_a/L_d$. This can be rewritten as $h_E \sim (L_a W_E/\nu_1)L_y$, where W_E and L_y are the amplitude and longitudinal scale of the Ekman pumping respectively. Another estimate of h_E in the ACC thermocline can be found in Karsten et al. (2002), and it is given by $h_E \sim \text{const} \times (f_o/F_{\text{so}})^{1/2} W_E L_y$. There, F_{so} is a prescribed surface buoyancy flux, which is related to the buoyancy difference $\Delta T = \text{const} \times F_{\text{so}}/W_E$. Therefore, in Karsten et al. (2002), $h_E \sim \text{const} \times (f_o W_E/\Delta T)^{1/2} L_y$, which is equivalent to the scaling of the classical thermocline theories obtained by Luyten et al. (1983) and Welander (1971). Our scaling differs qualitatively from Karsten et al. (2002) in that it explicitly relates the depth of the thermocline to the strength of the baroclinic eddies.

c. Surface layer thickness

The diabatic variations of the surface boundary layer depth are included in the entrainment rate w^*. In steady state, mass conservation in the surface layer implies

$$\partial_y \Psi + \partial_y \Psi^{\text{eddy}} = w^* \equiv \frac{1}{t_{\text{adj}}}(h_1^{\text{eq}} - h_1). \tag{30}$$

For $t_{\text{adj}} = 6$ months, the dominant balance in the surface layer depth, h_1, leads to approximately zero diabatic mass flux, $w^* \sim 0$ so that

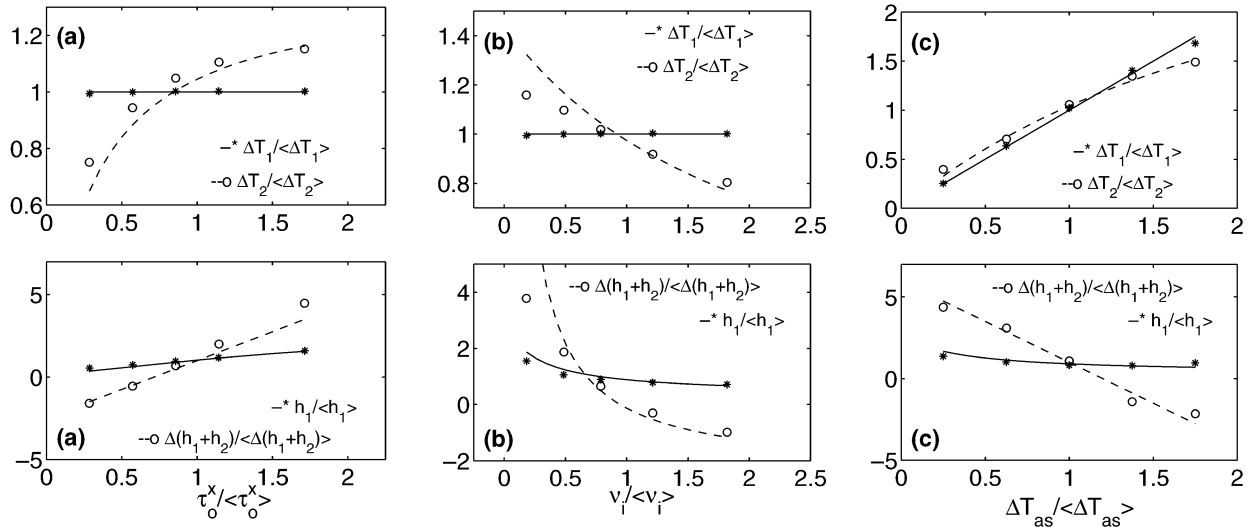

FIG. 7. Sensitivity of the layer temperatures and thicknesses to (a) the amplitude of the wind stress (τ_o^x), (b) the value of the eddy diffusivities (ν_i), and (c) the amplitude of the atmospheric temperature gradient (ΔT_{as}). All of the variables have been normalized by their corresponding solution-set averages: (a) $\langle \tau_o^x \rangle = 0.175$ N m^{-2}, $\langle \Delta T_1 \rangle = 12.2$°C, $\langle \Delta T_2 \rangle = 9.3$°C, $\langle h_1 \rangle = 230.0$ m, and $\langle \Delta(h_1 + h_2) \rangle = -150.4$ m; (b) $\langle \nu_i \rangle = 1650.0$ m^2 s^{-1}, $\langle \Delta T_1 \rangle = 12.2$°C, $\langle \Delta T_2 \rangle = 9.8$°C, $\langle h_1 \rangle = 262.4$ m, and $\langle \Delta(h_1 + h_2) \rangle = -246.7$ m; (c) $\langle \Delta T_{as} \rangle = 12.2$°C, $\langle \Delta T_1 \rangle = 12.0$°C, $\langle \Delta T_2 \rangle = 9.4$°C, $\langle h_1 \rangle = 280.6$ m, and $\langle \Delta(h_1 + h_2) \rangle = -151.1$ m. The upper panels contain the variations in the layer temperature gradients (ΔT_i) integrated over the interval $y = 1500$ km to $y = 3000$ km. The lower panels contain the variations in the surface layer thickness (h_1) averaged over the same interval. The circles and asterisks are the model solutions; the lines indicate the scaling relations (22), (29), (32), and (35). The scaling parameter in (35) has been taken to be $s = 0.45$.

$$h_1 \sim h_1^{\text{eq}}. \tag{31}$$

Using the definition of h_1^{eq} given in (18) and our previous estimate of the ocean temperatures in (29), Eq. (31) becomes

$$h_1 \sim \frac{H_1 H}{H_1 + H} \tag{32}$$

with

$$H_1 \equiv C_o \frac{2}{g\alpha_o} \frac{(\tau_o^x/\rho_o + u_{\text{ss}}^2)(1 + 4L_a/L_d)}{(T_{\text{as}} - T_D)}.$$

Therefore h_1 is set by a balance between the kinetic energy generated by the wind and the potential energy of the mean stratification. A stronger wind produces more turbulent activity and, therefore, a deeper mixed layer, while a stronger eddy response in the surface layer produces an increase in the stratification and a shallower mixed layer.

d. Upper-ocean thickness

By mass conservation, the upper-ocean's depth has a constant average. However, its latitudinal gradient is rather sensitive to the choice of atmospheric forcing and model parameters. A scaling estimate for the latitudinal variations of the upper ocean's depth can be derived using total mass conservation,

$$\Psi_T = -\Psi_T^{\text{eddy}}, \tag{33}$$

which always holds in steady state. Here, Ψ_T and Ψ_T^{eddy} denote ψ and ψ^{eddy} at $z = -h_1 - h_2$ respectively: Ψ_T^{eddy} is defined in (12), while Ψ_T consists of the input of momentum by the wind ($-\gamma f \tau^x/\rho_o$) minus the sink of momentum due to friction. Assuming for simplicity that the friction term in the total mean transport is proportional to the wind forcing term, Eq. (33) becomes

$$-s\frac{\tau^x}{f\rho_o} \sim \nu_2 \left[\partial_y (h_1 + h_2) + \frac{h_1 + h_2}{2} \frac{\partial_y T_2}{(T_2 - T_D)} \right], \tag{34}$$

where $\gamma f \sim 1/f$, s is some scaling constant between 0 and 1, and h_2 has been approximated by $(h_1 + h_2)$ in the definition of Ψ_T^{eddy}.

Using (28) and setting $(h_1 + h_2) \sim H$ as well as $f \sim -f_o$, and $\tau^x \sim \tau_o^x$, we obtain an approximate expression for the averaged latitudinal variation of $(h_1 + h_2)$ given by

$$\partial_y (h_1 + h_2) \sim \frac{H}{2L_a} \left(-1 + \frac{2s\tau_o^x L_a}{H f_o \rho_o \nu_2} \right). \tag{35}$$

In summary, the latitudinal variation of the upper ocean's depth, grows with τ_o^x/ν_2 in a similar fashion as the latitudinal variation of the thermocline temperature grows with τ_o^x/ν_1. Since both $\partial_y(h_1 + h_2)$ and $\partial_y T_2$ contribute to the integrated pressure gradient that is balancing the input of momentum into the layer, as the wind becomes weaker and the atmospheric temperature gradient becomes stronger, $\partial_y(h_1 + h_2)$ will change sign. In the limit of zero wind $\partial_y(h_1 + h_2)$ is mostly balancing a term proportional to $(h_1 + h_2)\partial_y T_2/(T_2 - T_D)$, which, following our simplified scaling estimate, is $-H/(2L_a)$.

The lower panels of Figs. 7a–c show the sensitivity of h_1 and $\partial_y(h_1 + h_2)$ to variations in the wind stress (Fig. 7a), the eddy diffusivity (Fig. 7b), and the atmospheric temperature gradient (Fig. 7c). We have followed the same procedure as in the analysis of the sensitivity of $\partial_y T_i$. The asterisks and circles correspond to the model solutions and the lines denote the predictions of the scaling theory (32) and (35). Here, h_1 and $\partial_y(h_1 + h_2)$ are, respectively, averaged and integrated over the interval $y = 1500$ km to $y = 3000$ km. The scaling constant, s, is adjusted to the value $s = 0.45$ that gives the best fit, implying that friction reduces the total meridional transport Ψ_T to half of the Ekman flow.

Using the leading order estimates for the layer temperatures and thicknesses discussed above, we can derive a scaling for the vertical stratification. For example, since both $(T_1 - T_2)$ and $(h_1)^{-1}$ increase with weaker winds, stronger eddies, and larger atmospheric temperature gradient, so does the vertical stratification at the base of the surface layer.

e. Zonal transport

A simple estimate of the total upper ocean zonal transport, U, can be obtained from geostrophy, where the larger contribution to the meridional pressure gradient yields

$$U \sim -\frac{g\alpha_o}{2f}\partial_y[(h_1 + h_2)^2(T_2 - T_D)]. \quad (36)$$

Using the mass conservation statement (33), the definitions of Ψ_T and ψ_T^{eddy}, and the estimate for $(T_2 - T_D)$, U scales as

$$U \sim \frac{\tau_o^x}{f_o \rho_o \nu_2}\left[\frac{\frac{g\alpha_o H}{f_o}(T_{\text{as}} - T_D)}{1 + \frac{4L_a}{L_d} + \frac{r_x}{f_o \nu_2}\frac{g\alpha_o H}{f_o}(T_{\text{as}} - T_D)}\right]. \quad (37)$$

The scaling (37) contains the effect of the wind, the eddies, and the atmospheric temperature gradient on the ACC transport. It grows approximately linearly with τ_o^x/ν_2 and decreases less than linearly with $\partial_y T_{\text{as}}$. This is confirmed by a sensitivity study (not shown).

Solutions from coarse-resolution ocean general circulation models confirm a dependence of the zonal transport in the Southern Ocean on the wind stress and the eddy diffusivity. Cai and Baines (1996) and Gent et al. (2001) find a correlation between the ACC, the meridional Ekman transport, and the deep density field. In both studies, the ACC transport increases with smaller eddy mixing and smaller horizontal viscosity. Furthermore, in Gent et al (2001), which includes the mesoscale eddy parameterization of Gent and McWilliams (1990), the main dependence on the eddy mixing comes from the isopycnal diffusivity parameter. Gnanadesikan and Hallberg (2000), also using a coarse-resolution global ocean model, find that the ACC transport increases with larger wind stress within the Southern Ocean. There is also observational evidence of a direct relationship between the wind stress and the ACC transport (Gille et al. 2001).

f. Residual meridional circulation and air–sea heat flux

In equilibrium, the transport of heat by the residual circulation balances the diabatic heat distribution into each layer. Ignoring horizontal diffusion, the steady-state layer heat balances are

$$+\Psi^R \partial_y T_1 + \partial_y \Psi^R (T_1 - T_2) H(+\partial_y \Psi^R) = F_s - F_1 \quad (38)$$

and

$$-\Psi^R \partial_y T_2 + \partial_y \Psi^R (T_1 - T_2) H(-\partial_y \Psi^R) = F_1 - F_2. \quad (39)$$

Here, $\Psi^R = \Psi + \Psi^{\text{eddy}}$ is the total residual transport within each layer. The sum of (38) and (39) provides the heat balance in the upper ocean, whose leading order is $T_1 \sim T_{\text{as}}$. Consideration of the next order balance, neglecting the smaller vertical diffusivity term, shows the relation between the air–sea heat flux and the residual circulation:

$$F_s \sim \partial_y[\Psi^R (T_{\text{as}} - T_2)]. \quad (40)$$

In the thermocline layer, (39) provides an expression for the residual transport as the net meridional flow necessary to balance the diabatic gradient of heat into the layer. Therefore, the strength and even the sign of the residual circulation (and hence of the air–sea heat flux) will depend closely on the parameterization of the process of vertical diffusion. Two scenarios are possible: 1) There is warming of the thermocline layer, $F_1 > F_2$. As a result, the residual circulation is negative and carries heat toward the pole, $\Psi^R < 0$. The resulting surface warming is accompanied by cooling to the atmosphere, $F_s < 0$. 2) There is cooling of the thermocline layer, $F_1 < F_2$. As a result, the residual circulation is positive and carries heat toward the equator, $\Psi^R > 0$. The resulting surface cooling is accompanied by warming from the atmosphere, $F_s > 0$. An example of type-1 solution is the control run. Making F_1 smaller than F_2 (e.g., by decreasing the value of μ_1 while keeping μ_2 constant) leads to solutions of type 2. Figure 8 shows the residual streamfunction and air–sea heat flux of a type-2 solution. In this run, $\mu_1 = 1 \times 10^{-6}$ m^2 s^{-1} and the other parameters are the same as those of the control run. The local cooling of the thermocline layer in the subpolar flank is balanced by equatorward advection of heat by the residual streamfunction and corresponding positive air–sea heat flux. A standard parameterization of the process of vertical diffusion described in (16), with $\mu_1 = \mu_2$ and typical ACC parameter values, leads to solutions of the type 1. For the rest of this section, we only consider solutions of this type.

In this model, the strength of the residual streamfunction and of the air–sea heat flux is constrained by

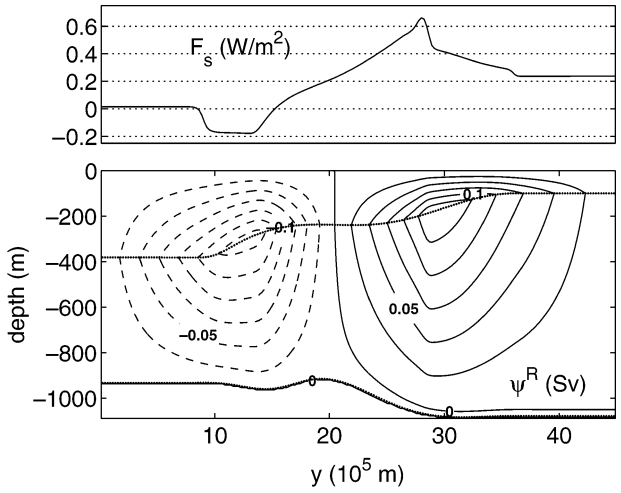

FIG. 8. (top) Air–sea heat flux and (bottom) residual streamfunction for a type-2 run with $\mu_1 = 1 \times 10^{-6}$. In the lower panel, the solid lines indicate positive values while the broken lines indicate negative values. The contour intervals are 0.025 Sv.

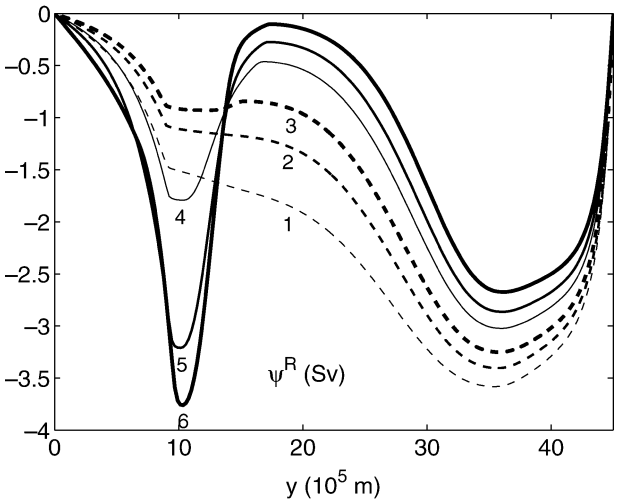

FIG. 9. Meridional profiles of Ψ^R for different values of the wind stress. Curves 1–6 correspond, respectively, to values of τ_o^x given by 0.05, 0.07, 0.1, 0.15, 0.2, and 0.3 N m^{-2}.

our definitions of the interior diabatic processes. An oceanic interior that is mostly adiabatic will have a weak residual overturning and air–sea heat flux. This is an important difference when comparing models in which the air–sea heat flux is prescribed. For instance, for the control run, the maximum of the residual circulation (away from the pole) is -3.0 Sv and F_s has a cooling peak of only -2.0 W m^{-2}. A scaling estimate of these magnitudes can be found in the appendix.

g. Polar overturning cell

Close to the pole, the horizontal and vertical stratification go to zero and it is no longer appropriate to use (39) to estimate the values of the residual streamfunction. In this region, the eddy transport, Ψ^{eddy}, is not dominated by the thermocline temperature gradient. Instead, Ψ^{eddy} is a delicate balance between the various terms compounding the parameterization of the eddy heat transport. Furthermore, the value of $(T_1 - T_2)$ depends on the onset of convective adjustment, and it is not possible to obtain a simple estimate of Ψ^R in the polar region.

The polar overturning cell may disappear in the presence of weak enough winds. Figure 9 shows the latitudinal profiles of Ψ^R for different values of τ_o^x and with the rest of the model parameters as in the control run. For small values of τ_o^x, the entrainment rate is negative throughout the interior of the channel and a residual polar cell does not develop. The residual circulation decreases slightly with the wind stress at all latitudes. For larger values of τ_o^x, there is positive entrainment at about $y = 2500$ km and, therefore, the residual circulation has two distinct peaks, a subpolar and a polar peak. The latter becomes more negative with larger values of the wind stress. Other important sensitivities of the magnitude of the polar residual circulation (not shown here) are a linear increase with the eddy diffusivity and a faster increase with the atmospheric temperature gradient.

h. The role of horizontal diffusion

So far, the horizontal diffusivity has been kept very small. However, it could be argued that, in the surface layer, there is horizontal mixing of temperature due to the interaction of turbulence and mesoscale eddies. When the lateral diffusivity in the surface layer is increased, the magnitude of the air–sea heat flux becomes larger to compensate for the increased diffusion of temperature while the transport by the residual circulation remains approximately unchanged. That is, even a very large increase in the surface lateral diffusivity, κ_1, produces only a small decrease in the surface temperature gradient, $\partial_y T_1$, which is, to leading order, still given by $\partial_y T_{\text{as}}$. This small change in $\partial_y T_1$ is, however, reflected in an increase in the amplitude of air–sea heat flux, which becomes more positive/negative in the equatorward/poleward half of the channel.

In order to quantify the relation between variations in the lateral diffusivity and variations in the amplitude of the air–sea heat flux, we have calculated the mean of the absolute value of F_s for different values of κ_1 from 10 to 1000 m^2 s^{-1}. The resulting points, $(\kappa_1, |F_s|)$, normalized by their respective means, are plotted in Fig. 10. The amplitude of the air–sea heat flux increases approximately linearly with the lateral diffusivity. The increase in air–sea flux is accompanied by an increase in the total poleward transport of heat, accomplished by the lateral diffusion.

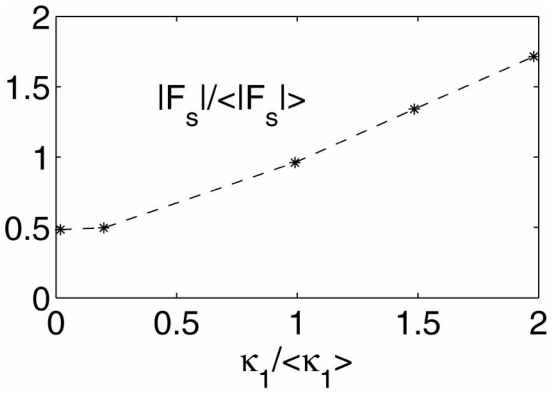

FIG. 10. Sensitivity of the amplitude of the air–sea heat flux ($|F_s|$) to the horizontal diffusivity in the surface layer (κ_1). All of the variables are normalized by their corresponding solution-set averages: $\langle\kappa_1\rangle = 505.0\ \mathrm{m^2\ s^{-1}}$ and $\langle|F_s|\rangle = 2.6\ \mathrm{W\ m^{-2}}$.

5. Summary and discussion

A simple model of a channel flow has been used to examine the equilibrium dynamics and thermodynamics of the ACC. It consists of a surface boundary layer and a thermocline layer separated by a turbulent interface. Each layer is characterized by variable, zonally averaged temperature and thickness. The effect of the mesoscale baroclinic eddies has been parameterized using an eddy-induced velocity field that transports heat poleward while decreasing the potential energy of the system. The ocean is forced by prescribed wind stress and relaxation to a prescribed atmospheric temperature.

Analyses of the model results suggest that the equilibrium thermal structure is mainly determined by the leading order balances of zero air–sea heat flux, zero entrainment rate, and zero residual circulation. The latitudinal gradients of the thermocline temperature and depth depend on two length scales: a dynamical length scale that reflects the competing effects of the wind and the eddies in the tilting of the isopycnals and the length scale of the imposed atmospheric temperature. The surface layer depth is set by a balance between the kinetic energy generated by the wind and the potential energy of the mean stratification. Stronger winds and weaker eddy diffusivity imply larger thermocline temperature and upper-ocean thickness gradients, deeper surface layer, and weaker stratification at the surface layer–thermocline interface. Meanwhile, a larger atmospheric temperature gradient implies a larger thermocline temperature gradient, a smaller upper-ocean depth gradient, and a stronger stratification at the surface layer–thermocline interface. The total geostrophic zonal transport corresponding to this thermal equilibrium structure depends approximately linearly on the wind stress and on the inverse of the eddy diffusivity.

Consideration of the next order balance shows a linear relationship between the air–sea heat flux and the magnitude of the residual overturning, which in turn depends on the processes of entrainment/detrainment, vertical diffusion, and, on the polar flank, convection. In this model the residual meridional circulation is characterized by two overturning cells, a subpolar cell and a narrower polar cell. The peak of the subpolar cell is determined by a balance between residual advection of temperature and vertical diffusion in the thermocline layer. The major sensitivities of the magnitude of this cell are an almost linear growth with the eddy diffusivity and a square-root dependence on the vertical diffusivity. The meridional cell is accompanied by cooling to the atmosphere at the poleward side of the cell compared to the equatorward side. This cooling is larger for weaker winds, stronger eddies, and larger atmospheric temperature gradients. On the other hand, the polar cell is controlled by entrainment cooling and convection. It appears for strong enough winds and increases with the wind stress, the eddy diffusivity, and the atmospheric temperature gradient. Since the ocean's interior is nearly adiabatic, the meridional residual circulation is of the order of a few Sverdrup. Therefore, the poleward transport of heat by the residual flow is very weak. In the absence of lateral diffusion this implies a correspondingly weak differential cooling to the atmosphere. This limitation on the meridional transport of heat by the ocean can be avoided by including significant ($\kappa_1 \sim \nu_1$) lateral diffusion in the surface layer. In this model, larger horizontal diapycnal mixing is mostly compensated by larger amplitude of the air–sea heat flux.

Previous analyses of the climatology of the ACC (Karsten et al. 2002; MR) have also made use of the zero-order balance between the mean and the eddy-induced circulations to arrive at scaling arguments for the stratification and transport in a mechanically and thermodynamically driven channel flow. Their solutions show the same competing role of the wind and the eddies in setting the buoyancy distribution in the ocean's interior. Stronger winds and weaker eddy transport efficiency imply larger baroclinic zonal transport and smaller vertical stratification. The specific power laws vary with the details of each model. The vertical discretization of buoyancy and the particular choice of the parameterizations of the eddy fluxes are especially important. The main difference between previous work and ours arrives when considering the next order balance. In our model, the meridional residual circulation and the air–sea heat flux are settled by the interior's ocean dynamics and depend on diabatic processes. In contrast, Karsten et al. (2002) and MR prescribe the buoyancy flux at the surface and consider the oceanic interior to be adiabatic. In Karsten et al. (2002), the residual streamfunction is assumed to scale proportionally to the Ekman transport. In MR a complete diagnosis of the strength of the residual streamfunction as the ratio between the imposed surface buoyancy flux and surface buoyancy gradient is possible because the latter quantities are prescribed, and a stronger residual

flow is supported by heat exchange at the open subpolar boundary.

In this work we have considered a closed system, focusing on the energy budget of the ACC alone. We believe that analyzing the mechanics of equilibration of a channel flow in a closed domain is essential for the understanding of the dynamics of the ACC, particularly considering the present incomplete knowledge of the meridional flow and surface fluxes in the Southern Ocean. Had we chosen to exchange mass and heat with the subtropics, the vertical structure of this exchange would have been limited by the current heavy vertical truncation of our model. For example, for an adiabatic interior, incoming heat from the subtropics would always require an equatorward residual flow in the thermocline layer and vice versa (since the model cannot produce two counterrotating cells one above the other). A formulation with a higher number of degrees of freedom in the vertical would be more appropriate when considering open lateral boundaries.

As mentioned in the introduction, reliable direct measurements of the air–sea heat flux and ocean heat transport in the Southern Ocean are currently not available. Using different atmospheric reanalysis, Trenberth and Caron (2001) and Trenberth et al. (2001) have compared several estimates of global air–sea heat fluxes and implied ocean heat transports. In their work, the implied zonal mean transport in the ACC region based upon surface fluxes derived from NCEP and ECMWF reanalyses is poleward and of the order of 0.5 PW. The same estimate is obtained with several coupled climate models without flux correction (HADCM3, CSM). On the other hand, surface fluxes from the NCEP assimilated model imply an poleward ocean heat transport of 2 PW while those from the ECMWF assimilated model imply an equatorward transport of the same magnitude. Using COADS surface fluxes produces an equatorward transport of a few petawatts across the Southern Ocean. In summary, the current estimates are unable to determine the sign of the heat transport in the ACC region, perhaps an indication that the latter is small.

Our work predicts that the meridional ocean heat transport and air–sea heat flux are small, on the order of 0.05 PW and 2 W m^{-2}, respectively. The hypothesis leading to this result is that a meridional circulation that returns throughout a weakly diabatic interior produces a weak meridional heat transport and a correspondingly weak differential cooling to the atmosphere. In a closed domain, any larger air–sea heat flux would be balanced in equilibrium by ocean heat transport that takes place through a larger diapycnal mixing than is consistent with the parameterized mixing rates used here. In an open domain with heat flux through the meridional boundaries, larger air–sea fluxes might occur, but then the controlling dynamics would be global in scale.

Acknowledgments. Funding for this research was provided by the National Science Foundation (OCE 96-33681 and 96-18126) and the Department of Energy (Climate Change Prediction Program). We are grateful to R.M. Samelson and two anonymous reviewers for their suggestions.

APPENDIX

Scaling of Residual Streamfunction and Air–Sea Heat Flux

An estimate of the peak of the residual circulation (away from the pole) is given by

$$\Psi_m^R = -\frac{F_{1m} - F_{2m}}{\partial_y T_{2m}}, \tag{A1}$$

where the subscript m refers to the values at the location where the magnitude of the residual circulation is maximum. Assuming that F_{1m} dominates over F_{2m},

$$\Psi_m^R \sim -\frac{F_{1m}}{\partial_y T_{2m}} = -\frac{\mu_1}{h_{1m}}\frac{(T_{1m} - T_{2m})}{\partial_y T_{2m}}. \tag{A2}$$

In the region of stronger residual flow, the Ekman circulation is small and $\Psi^R \sim \Psi^{\text{eddy}}$ so that

$$\Psi_m^R \sim -\nu_1\frac{(h_{1m} + h_{2m})}{2}\frac{\partial_y T_{2m}}{(T_{1m} - T_{2m})}. \tag{A3}$$

Therefore, combining (A2) and (A3), we obtain

$$\Psi_m^R \sim -\left(\mu_1\nu_1\frac{h_{1m} + h_{2m}}{2h_{1m}}\right)^{1/2}. \tag{A4}$$

Since the latitudinal variations in $h_1 + h_2$ are mostly localized on the poleward side of the channel, for simplicity we will take $h_{1m} + h_{2m} \sim H$. Also, h_{1m} is given by its equilibrium value, obtained by neglecting τ_o^x in (32). Last, assuming that $(T_{1m} - T_{2m})$ is proportional to its averaged value over the center of the channel, $(T_1 - T_2)$ [given by (29)], (A4) becomes

$$\Psi_m^R \sim -\sqrt{\mu_1\nu_1\frac{Hg\alpha_o}{4C_o u_{ss}^2}\frac{(T_{as} - T_D)}{(1 + 4L_a/L_d)}}. \tag{A5}$$

According to (A5), the residual circulation varies with the square root of the vertical diffusivity. This scaling is confirmed by the model solutions presented in the upper panels of Fig. A1 where Ψ_m^R is plotted versus $\mu_1 = \mu_2$. The asterisks correspond to the model solutions, the broken line follows the scaling (A5), and the solid line is the best linear fit on logarithmic scales with a slope of 0.44. Figure A2 shows Ψ_m^R versus wind stress (upper left panel), versus eddy diffusivity (upper central panel), and versus atmospheric temperature gradient (upper right panel). The strongest dependence, almost linear, is on the eddy diffusivity. In Fig. A1 the range of ν_i and ΔT_{as} is smaller than that used in Figs. 5 and 7. The lowest values in Figs. 5 and 7 ($\nu_i = 300$ m^2 s^{-1}

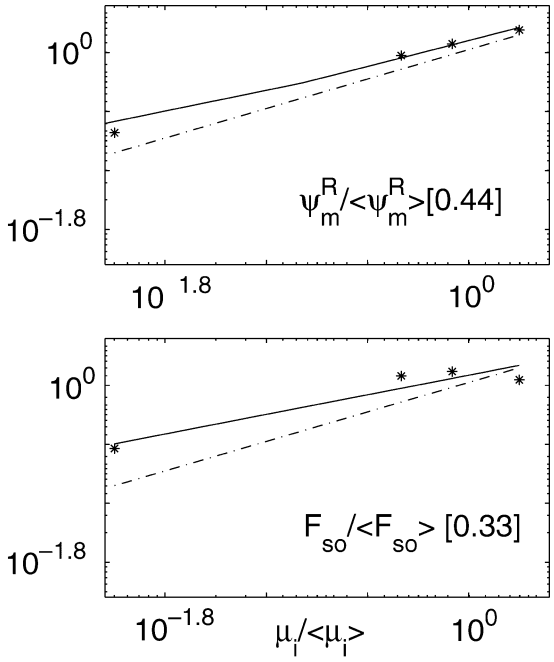

FIG. A1. Sensitivity of the magnitude of the residual circulation away from the Pole and of the air–sea heat flux to the value of the vertical diffusivities (μ_i). The plots are on logarithmic scale with variables normalized by their corresponding solution-set averages: $\langle\mu_i\rangle = 2.2555 \times 10^{-5}$ m^2 s^{-1}, $\langle\Psi_m^R\rangle = 3.2$ Sv, and $\langle F_{so}\rangle = -0.8$ W m^{-2}. (top) The variations in the equatorward peak of the residual meridional streamfunction (Ψ_m^R); (bottom) the variations in the air–sea heat flux averaged over the interval $y = 1500$ km to $y = 3000$ km, (F_{so}). The asterisks are the model solutions while the broken lines are the scalings (A5) and (A7). The solid lines follow the best linear fit whose slope appears in the legends inside brackets.

and $\Delta T_{as} = 4$°C) are omitted here because those model solutions belong to type 2 (cf. Fig. 8).

In summary, both the residual circulation and the vertical temperature difference ($T_1 - T_2$) decrease when the wind stress increases so that stronger winds produce weaker oceanic transport of heat. This is contrary to our understanding of the mechanical response of the ocean circulation at other latitudes.

The scaling of the air–sea heat flux around the center of the channel, F_{so}, follows from (40), which can be approximately expressed as

$$F_{so} \sim \frac{\Psi_m^R(T_{as} - T_2)}{L_a}. \tag{A6}$$

Using the scaling (A5) we obtain

$$F_{so} \sim -\frac{1}{L_a}\left(\mu_1\nu_1\frac{Hg\alpha_o}{4C_o u_{ss}^2}\right)^{1/2}\left[\frac{(T_{as} - T_D)}{(1 + 4L_a/L_d)}\right]^{3/2}. \tag{A7}$$

The sensitivity curves of F_{so} are presented in the lower panels of Figs. A1 and A2. Figure A1 shows that the variations of the air–sea heat flux with μ_1 are slower than $\sqrt{\mu_1}$, specially for the higher values of μ_1. This is because, for large enough vertical diffusivity, F_2 is not negligible in comparison with F_s, and (40) is not longer valid. As for the other parameters, F_{so} becomes more negative with stronger eddies, weaker winds and larger atmospheric temperature gradients.

Previous analyses of the ACC overturning cell in Karsten et al. (2002) and MR have prescribed air–sea heat flux F_{so} and have excluded turbulent entrainment and vertical diffusivity. In this framework, the residual circulation at the base of a surface mixed layer of buoyancy

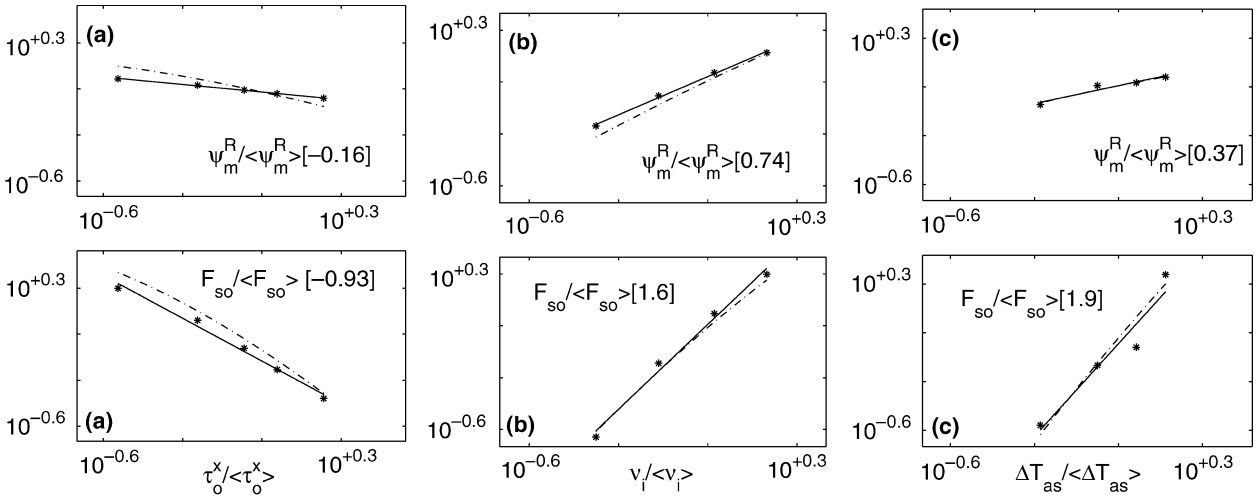

FIG. A2. Sensitivity of the magnitude of the residual circulation away from the pole and of the air–sea heat flux to (a) the magnitude of the wind stress (τ_o^x), (b) the value of the eddy diffusivities (ν_i), and (c) the amplitude of the atmospheric temperature gradient (ΔT_{as}). All the plots are on logarithmic scale with variables normalized by their corresponding solution-set averages: In (a) $\langle\tau_o^x\rangle = 0.175$ N m^{-2}, $\langle\Psi_m^R\rangle = 3.1$ Sv, and $\langle F_{so}\rangle = -1.4$ W m^{-2}; (b) $\langle\nu_i\rangle = 1900.0$ m^2 s^{-1}, $\langle\Psi_m^R\rangle = 3.6$ Sv, and $\langle F_{so}\rangle = -1.7$ W m^{-2} ; and (c) $\langle\Delta T_{as}\rangle = 14.4$°C, $\langle\Psi_m^R\rangle = 3.0$ Sv, and $\langle F_{so}\rangle = -1.7$ W m^{-2}. (top) The equatorward peak of the residual meridional streamfunction (Ψ_m^R); (bottom) the air-sea heat flux averaged over the interval $y = 1500$ km to $y = 3000$ km, (F_{so}). Here ΔT_{as} is a latitudinal gradient integrated over the same interval. The asterisks correspond to the model solutions; the broken lines corresponds to the scalings (A5) and (A7). The solid lines follow the best linear fit whose slope appears in the legends inside brackets.

T is given by $\Psi^R \sim F_s L_y/\Delta T$. Such a system can have a nonzero residual circulation because it is open at the equatorial boundary where heat is exchanged below the surface. With this setup, MR can specify both the buoyancy gradient and the buoyancy flux of the surface layer, leading to a complete diagnosis of the magnitude of the residual flow. In contrast, ΔT is not prescribed in Karsten et al. (2002) and a scaling estimate for Ψ^R is required. Neglecting friction and Reynolds stresses in the zonal momentum balance, the residual overturning is defined as the sum of Ekman plus eddy-induced circulations. The eddy heat flux is parameterized as downgradient diffusion with eddy diffusivity ν. Their major assumption is to consider that the eddy circulation that approximately balances the Ekman flow scales proportionally to the interior value of ν, ν_I. Thus the residual circulation scales as $\Psi^R \sim (\nu/\nu_I - 1)\tau_o^x/(f_o\rho_o)$, where ν/ν_I is a tunable parameter.

In our work, F_s is not prescribed but it is linearly related to the residual circulation, which in turn depends on diabatic processes. Therefore, our scaling of Ψ^R differs from that of previous work. In particular, the magnitude of Ψ^R, (and therefore of F_s) is constrained by the strength of the diabatic processes. This is in contrast with MR and Karsten et al. (2002) in which the magnitude of Ψ^R can be controlled directly by changing the magnitude of the imposed air–sea heat flux MR or the magnitude of the imposed wind stress (Karsten et al. 2002).

REFERENCES

Andrews, D., J. Holton, and C. Leovy, 1987: *Middle Atmosphere Dynamics.* Academic Press, 489 pp.

Cai, W., and P. Baines, 1996: Interactions between thermohaline and wind driven circulations and their relevance to the dynamics of the Antarctic Circumpolar Current in a coarse resolution global ocean general circulation model. *J. Geophys. Res.,* **101,** 14 073–14 093.

Danabasoglu, G., J. McWilliams, and P. Gent, 1994: The role of mesoscale tracer transports in the global ocean circulation. *Science,* **264,** 1123–1126.

daSilva, A., C. Young, and S. Levitus, 1994: *Algorithms and Procedures.* Vol. 1, *Atlas of Surface Marine Data,* NOAA Atlas NESDIS 6, U.S. Department of Commerce, 83 pp.

Deacon, G., 1984: *The Antarctic Circumpolar Ocean.* Cambridge University Press, 180 pp.

Doos, K., and D. Webb, 1994: The Deacon cell and the other meridional cells of the Southern Ocean. *J. Phys. Oceanogr.,* **24,** 429–442.

Gent, P., and J. McWilliams, 1990: Isopycnal mixing in ocean circulation models. *J. Phys. Oceanogr.,* **20,** 150–155.

——, J. Willerbrand, and T. M. J. McWilliams, 1995: Parameterizing eddy-induced tracer transports in ocean circulation models. *J. Phys. Oceanogr.,* **25,** 463–474.

——, W. Large, and F. Bryan, 2001: What sets the mean transport through Drake Passage? *J. Geophys. Res.,* **106,** 2693–2712.

Gille, S., 2003: Float observations of the Southern Ocean. Part I. Estimating mean fields, bottom velocities, and topographic steering. *J. Phys. Oceanogr.,* **33,** 1167–1181.

——, D. Stevens, R. Tokmakian, and K. Heywood, 2001: Antarctic Circumpolar Current response to zonally averaged winds. *J. Geophys. Res.,* **106,** 2743–2759.

Gnanadesikan, A., and R. Hallberg, 2000: On the relationship of the Circumpolar Current to Southern Hemisphere winds in coarse-resolution ocean models. *J. Phys. Oceanogr.,* **30,** 2013–2034.

Gordon, A., E. Molinelli, and T. Baker, 1982: *Southern Ocean Atlas.* Columbia University Press, 35 pp. and 248 plates.

Ivchenko, V., K. Richards, and D. Stevens, 1996: The dynamics of the Antartic Circumpolar Current. *J. Phys. Oceanogr.,* **26,** 753–774.

Johnson, G., and H. Bryden, 1989: On the size of the Antartic Circumpolar Current. *Deep-Sea Res.,* **36A,** 39–53.

Josey, S., E. Kent, and P. Taylor, 1999: New insights into the ocean heat budget closure problem from analysis of the SOC air–sea flux climatology. *J. Climate,* **12,** 2856–2880.

Karsten, R., and J. Marshall, 2002: Constructing the residual circulation of the ACC from observations. *J. Phys. Oceanogr.,* **32,** 3315–3327.

——, H. Jones, and J. Marshall, 2002: The role of eddy transfer in setting the stratification and transport of a circumpolar current. *J. Phys. Oceanogr.,* **32,** 39–54.

Kraus, E., and J. Turner, 1967: A one-dimensional model of the seasonal thermocline. Part II: The general theory and its consequences. *Tellus,* **19,** 98–106.

Luyten, J., J. Pedlosky, and H. Stommel, 1983: The ventilated thermocline. *J. Phys. Oceanogr.,* **13,** 292–309.

Marshall, D., 1997: Subduction of water masses in an eddying ocean. *J. Mar. Res.,* **55,** 201–222.

Marshall, J., and T. Radko, 2003: Residual-mean solutions for the Antarctic Circumpolar Current and its associated overturning circulation. *J. Phys. Oceanogr.,* **33,** 2341–2354.

——, H. Jones, R. Karsten, and R. Wardle, 2002: Can eddies set ocean stratification? *J. Phys. Oceanogr.,* **32,** 26–38.

McCreary, J., and P. Lu, 1994: Interaction between the subtropical and equatorial ocean circulations. *J. Phys. Oceanogr.,* **24,** 466–497.

McWilliams, J., W. Holland, and J. Chow, 1978: A description of numerical Antartic Circumpolar Currents. *Dyn. Atmos. Oceans,* **2,** 213–291.

Nowlin, W., and J. Klinck, 1986: The physics of the Antartic Circumpolar Current. *Rev. Geophys.,* **24,** 469–491.

Olbers, D., V. Gouretski, G. Seiss, and J. Schroter, 1992: *Hydrographic Atlas of the Southern Ocean.* Alfred Wegener Institute, 82 pp. [Available online at http://www.awi-bremerhaven.de/Atlas/SO/Deckblatt.html.]

Rintoul, S., C. Hughes, and D. Olbers, 2001: The Antarctic Circumpolar Current System. *Ocean Circulation and Climate,* Academic Press, 271–302.

Schmitz, W., 1996: On the World Ocean circulation, Vol. II. Tech. Rep. WHOI-96-08, Woods Hole Oceanographic Institution.

Speer, K., S. Rintoul, and B. Sloyan, 2000: The diabatic Deacon cell. *J. Phys. Oceanogr.,* **30,** 3212–3222.

Treguier, A., I. Held, and V. Larichev, 1997: Parameterization of quasigeostrophic eddies in primitive equation ocean models. *J. Phys. Oceanogr.,* **27,** 567–580.

Trenberth, K., and J. Caron, 2001: Estimates of meridional atmosphere and ocean heat transports. *J. Climate,* **14,** 3433–3443.

——, ——, and D. Stepaniak, 2001: The atmospheric energy budget and implications for surface fluxes and ocean heat transports. *Climate Dyn.,* **17,** 259–276.

Welander, P., 1971: The thermocline problem. *Philos. Trans. Roy. Soc. London,* **A270,** 415–421.

Zilitinkevich, S., and D. Mironov, 1996: A multi-limit formulation for the equilibrium depth of a stably stratified boundary layer. *Bound.-Layer Meteor.,* **81,** 325–351.